Check for updates

Magnetically Actuated Artificial Microswimmers as Mobile Microparticle Manipulators

Jake Buzhardt
Department of Mechanical Engineering,
Clemson University,
Clemson, SC 29630
e-mail: jbuzhar@g.clemson.edu

Phanindra Tallapragada[1]
Department of Mechanical Engineering,
Clemson University,
Clemson, SC 29630
e-mail: ptallap@clemson.edu

Microscale swimming robots have been envisaged for many biomedical applications such as targeted drug delivery, where the microrobot will be expected to navigate in a fluid environment while carrying a payload. We show that such a payload does not have to be physically bound to the swimmer, but may be instead manipulated by the microrobot through hydrodynamic interaction. We consider a magnetically actuated artificial microswimmer, whose locomotion induces a disturbance velocity field in the fluid, which moves a cargo particle in its vicinity. The problem investigated in this paper is therefore one of coupled locomotion-manipulation of two bodies in a fluid. The swimmer is actuated by a uniform, rotating magnetic field of constant strength leading to net motion in the direction perpendicular to the plane of rotation if the frequency associated with the periodic magnetic field is above a critical frequency. Below this critical frequency, the swimmer tumbles in place without net locomotion. Controlled motion of the particle and swimmer is achieved by switching the planes of rotation of the magnetic field and the frequency of the magnetic field above and below the critical frequency. The results of this paper show that microswimmers can be utilized as mobile manipulators of microparticles in a fluid.
[DOI: 10.1115/1.4046581]

Keywords: biological systems applications, medical robotics, modeling, microswimmers

1 Introduction

Microrobots that can swim and navigate in microchannels hold great potential for many medical applications such as targeted drug delivery, cellular manipulation, and diagnostics [1–3]. These microrobots can derive their propulsive ability via magnetic [4–6], electric [7], acoustic [8], optical [9], or chemical [10,11] actuation. In many applications, these microrobots are expected to carry a payload that by itself cannot be propelled or steered easily. Common solutions require that the cargo particles be bonded to the microrobot and then be released by the robot when required. This can pose limitations on the cargo that can be carried. An alternative approach is to manipulate particles without contact by exploiting the hydrodynamic interaction between the microrobot and the particle. In essence, the microrobot becomes a mobile contactless micromanipulator.

In this paper, we investigate through computations the ability of a magnetically actuated microswimmer to steer a nonmagnetic particle of a comparable length scale in its neighborhood in a contactless manner. Magnetic fields with small magnitude, but time-periodic direction induce a torque on magnetized particles, thus causing the particles to rotate. For bodies possessing an appropriate asymmetry, this rotational motion can lead to propulsion [12]. The propulsive speed or lack thereof is a function of the frequency of the magnetic field, and the direction of propulsion depends on the direction of rotation of the magnetic field. Therefore, control of the direction and frequency of field rotation enables the steering of a magnetic swimmer. We show that the swimmer may be used as a mobile microparticle manipulator, steering the nonmagnetic cargo particle in a desired direction, as steering the swimmer effectively controls the fluid velocity field experienced by the cargo particle. The equations governing this interaction form a driftless control affine system as a consequence of the lack of inertia in a Stokes flow. This observation is then used to determine a magnetic field input to generate controlled motion of both the magnetic swimmer and the passive particle in arbitrary directions.

2 Modeling of the Swimmer–Particle Interaction

The motion of the artificial microswimmers and particles considered in this work is described by very small length and velocity scales, and thus, the corresponding fluid motion is governed by the Stokes equations. The linearity of the Stokes equations implies that the forces and torques acting on a body are linearly related to the velocity and angular velocity of the body [12,13]; this relationship is known as the mobility relationship.

The geometry of the artificial swimmer considered in this paper consists of three spheres, rigidly connected with a 90 deg bend as shown in Fig. 1(*a*). This body is chosen both for the structure of its mobility matrix and for its ease of fabrication [5]. The swimmer is to be driven by a torque produced by a magnetic field, with the external forcing $\mathbf{F}^e = \mathbf{0}$. Thus, to achieve a translational motion, it is necessary that the matrix coupling torque to translational velocity, denoted $\mathbf{C}$, be nonzero. One of the simplest geometric conditions for a body to have a nonzero coupling matrix $\mathbf{C}$ is that the body have two mutually perpendicular planes of symmetry, but not three [12]. The mobility matrix associated with this particular geometry has been derived previously in Refs. [14–16].

In cases where multiple bodies are present in a fluid, it is also necessary to consider the hydrodynamic coupling between bodies. The relationship between the forcings and the body velocities is still linear in this case and is represented using a grand mobility matrix. In this work, we consider the motion of a particle in the presence of a microswimmer, so the grand mobility relationship is given by

$$\begin{pmatrix} \mathbf{V}_s \\ \mathbf{V}_p \\ \boldsymbol{\Omega}_s \\ \boldsymbol{\Omega}_p \end{pmatrix} = \begin{pmatrix} \mathbf{K}_{ss} & \mathbf{K}_{sp} & \mathbf{C}_{ss} & \mathbf{C}_{sp} \\ \mathbf{K}_{ps} & \mathbf{K}_{pp} & \mathbf{C}_{ps} & \mathbf{C}_{pp} \\ \mathbf{C}_{ss}^{\mathsf{T}} & \mathbf{C}_{sp}^{\mathsf{T}} & \mathbf{M}_{ss} & \mathbf{M}_{sp} \\ \mathbf{C}_{ps}^{\mathsf{T}} & \mathbf{C}_{pp}^{\mathsf{T}} & \mathbf{M}_{ps} & \mathbf{M}_{pp} \end{pmatrix} \begin{pmatrix} \mathbf{F}_s^e \\ \mathbf{F}_p^e \\ \mathbf{T}_s^e \\ \mathbf{T}_p^e \end{pmatrix} \tag{1}$$

where the subscripts s and p indicate the particle and the swimmer, respectively. In the case of a single rigid body, it is often convenient

[1]Corresponding author.

Manuscript received December 8, 2019; final manuscript received February 20, 2020; published online March 4, 2020. Assoc. Editor: Jordan M. Berg.

Copyright © 2020 by ASME

Downloaded from http://asmedigitalcollection.asme.org/lettersdynsys/article-pdf/1/1/011016/6519920/aldsc_1_1_011016.pdf by Clemson University user on 16 November 2021

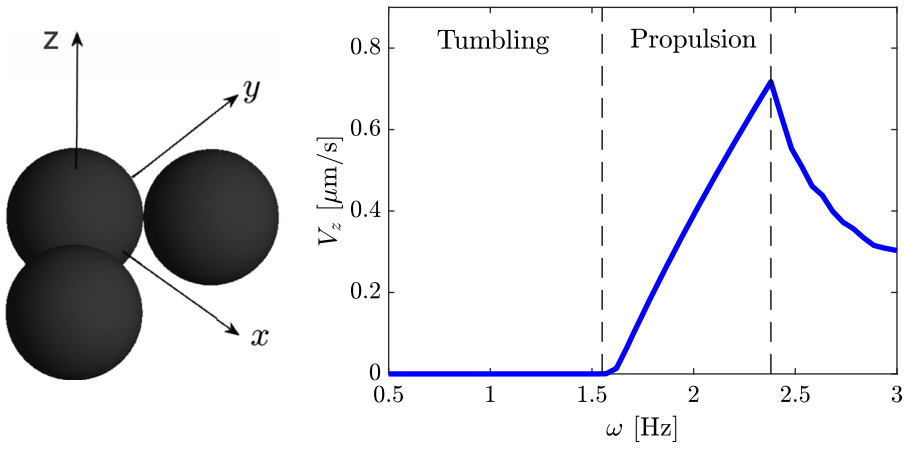

Fig. 1 (*a*) Three-sphere artificial microswimmer considered in this work, shown in the axes of the body-fixed frame of reference and (*b*) dependence of swimmer propulsion velocity on driving frequency ω of the rotating magnetic field.

to represent these dynamics in a body-fixed frame of reference, as the submatrices **K**, **C**, and **M** are dependent only on the body geometry and thus remain constant in a body-fixed frame. However, in the case of multiple interacting bodies, each of the terms in this matrix depends on the relative position and orientation of each body. Therefore, it is more convenient to define these matrices in a common, spatially fixed reference frame.

To define the grand mobility matrix for this system, we implement the Stokesian dynamics algorithm [17–19], which has been recently used to compute the grand mobility tensor of a collection of swimmers [20]. The method is especially suited for systems composed of spheres moving in a viscous fluid.

This algorithm relies on the multipole expansion of the disturbance velocity field due to each sphere along with the Faxén relationships to compute the effect of this field on all other spheres in the system. Full details of this derivation along with the expressions for the elements of this many-sphere grand mobility matrix are given in Ref. [18].

To condense this matrix describing the motion of all spheres (denoted by α) into a matrix describing the motion of a rigid body composed of spheres (denoted by *A*), we apply the conditions of rigid body motion that $\mathbf{V}_\alpha = \mathbf{V}_A + \mathbf{\Omega}_A \times \mathbf{r}_{\alpha A}$ and $\mathbf{\Omega}_\alpha = \mathbf{\Omega}_A$. Here, $\mathbf{r}_{\alpha A}$ is the vector from a chosen reference of the rigid body *A* to the center of the sphere α. Further, the quasi-static conditions of rigid body motion in a Stokes flow require that all hydrodynamic forcings exactly balance with the external forcings.

Further details of this method are found in Ref. [19]. The result of the calculation outlined here is a grand mobility matrix of the same form as shown in Eq. (1) that gives the hydrodynamic coupling between the artificial microswimmer and the spherical particle. Since this matrix is dependent on the position and the orientation of both bodies, in simulation, it is updated at each time step.

We consider the propulsion of a body by an externally applied magnetic field. For this, the magnetization of the body is described by a magnetic moment vector **m**, defined in a body-fixed frame of reference and thus assumed to remain constant. The externally applied torque acting on the body of the artificial swimmer is then given by $\mathbf{T}_s^e = (\mathbf{R}^\mathsf{T}\,\mathbf{m}) \times \mathbf{B}$, where **B** is the applied magnetic field in the spatially fixed frame of reference and $\mathbf{R}^\mathsf{T}$ is the rotation transformation from the body-fixed frame to the spatially fixed frame. The torque $\mathbf{T}_s^e$ is the only external actuation imparted to the system, as no forces are applied and the spherical particle is not magnetized, so it is unaffected by the magnetic field.

Since the dynamics are dependent on the body orientation relative to the spatially fixed reference frame, it is necessary to parameterize this orientation of the body. For this, we adopt the standard *ZXZ* Euler angles [21], and the transformation **R** from the spatially fixed frame to the body-fixed frame is given by $\mathbf{R} = \mathbf{R}_z(\text{psi})\,\mathbf{R}_x(\theta)\,\mathbf{R}_z(\phi)$, where $\mathbf{R}_x$ and $\mathbf{R}_z$ are the matrices representing the rotation by the given angles about the *x* and *z* axes, respectively, of the body-fixed frame. Since these matrices are orthogonal, the inverse transformation from the body-fixed frame to the spatially fixed frame is given by $\mathbf{R}^{-1} = \mathbf{R}^\mathsf{T}$, where the superscript T indicates matrix transposition.

2.1 Control System Formulation. Considering the grand mobility formulation along with the necessary rigid body constraints and kinematics, we have defined a nonlinear dynamical control system of the form

$$\frac{d\boldsymbol{\xi}}{dt} = \mathbf{f}(\boldsymbol{\xi}, \boldsymbol{\upsilon}) \tag{2}$$

where the state vector is $\boldsymbol{\xi} \triangleq \left(\mathbf{X}_s^\mathsf{T}, \mathbf{X}_s^\mathsf{T}, \mathbf{\Theta}_s^\mathsf{T}, \mathbf{\Theta}_p^\mathsf{T}\right)^\mathsf{T}$. Here, the vectors **X** represent the respective positions of the artificial swimmer and the passive particle and the vectors **Θ** are vector representations of the *ZXZ* Euler angles, all defined relative to a spatially fixed frame of reference.

It has been previously shown both experimentally and theoretically that propulsion of the artificial swimmer can be achieved by applying a magnetic field that rotates steadily in the spatially fixed frame. This form of input results in a translational motion of the swimmer along the axis of rotation of the magnetic field for some range of rotation frequencies. In this work, we seek to show that the swimmer and the passive particle can be steered along any arbitrary direction. So, we take the applied magnetic field to be of the form

$$\mathbf{B}(t) = \mathbf{R}_l(\gamma) \cdot B \cdot (\cos\omega t,\ \sin\omega t,\ 0)^\mathsf{T} \tag{3}$$

where the matrix $\mathbf{R}_l(\gamma)$ is a rotation about an axis *l* by an angle γ and ω is the frequency of rotations. Without loss of generality, in this paper, we consider only the case where the axis *l* is chosen to be the spatially fixed *y*-axis. This allows the magnetic field to be directed along any vector in the *xz*-plane. With this, the control inputs are taken to be $\boldsymbol{\upsilon} \triangleq (\gamma, \omega)^\mathsf{T}$.

3 Simulation Results

With the particle dynamics well defined and the control system formulated, we are able to simulate the dynamics of the

Downloaded from http://asmedigitalcollection.asme.org/lettersdynsys/article-pdf/1/1/011016/6519920/aldsc_1_1_011016.pdf by Clemson University user on 16 November 2021

swimmer–particle system. Starting from an initial state, the dynamics are integrated forward in time using MATLAB's built-in variable-order differential equation solver, ODE113.

The numerical values of the parameters used for the simulations shown in this work are outlined as follows. The magnetic moment vector is defined in the body-fixed frame of reference as $\mathbf{m} = m(0, \frac{\sqrt{2}}{2}, \frac{\sqrt{2}}{2})^{\mathbf{T}}$ with a magnitude $m = 4.0 \times 10^{-15}$ N m/T. The strength of the magnetic field is held constant at $B = 5.0 \times 10^{-3}$ T. The artificial microswimmer is composed of rigidly linked magnetic spheres of radius $a = 2.25\ \mu$m, with an internal bend angle of 90 deg. Passive spheres considered in these simulations are also of radius $a = 2.25\ \mu$m. These numerical values are chosen based on the values reported in the experimental works on this subject, specifically Ref. [5].

Before considering the dynamics of swimmer–particle interaction, we briefly explain the dynamics of a single swimmer, propelled by a rotating magnetic field. It is a well-known result that magnetically actuated artificial swimmers only exhibit meaningful locomotion for a certain range of driving frequencies of the oscillating field [22–24]. Specifically, there exist three distinct frequency-dependent motion regimes. At low frequencies, the magnetic moment vector tends to follow the magnetic field, resulting in a *tumbling* motion of the swimmer, in which the body rotates in place but experiences very little net propulsion. At slightly larger frequencies, the swimmer begins to exhibit propulsion by precessing about an axis. Finally, there exists a second critical frequency beyond which the magnetic moment vector of the swimmer is unable to follow the rotating magnetic field. This critical frequency is commonly known as the *step-out* frequency. In this regime, swimmer propulsion falls off rapidly and the swimmer dynamics become difficult to predict or control. The dependence of the swimmer velocity on the driving frequency is illustrated in Fig. 1(*b*). These distinct regimes have been shown previously for different body geometries, both experimentally and theoretically, in many works (see, for example, Refs. [15,22]).

We will show that while the swimmer does not exhibit meaningful propulsion in the tumbling regime, the rotation of the body as the magnetic moment vector follows the magnetic field generates a rotating fluid velocity field that is useful for stirring the fluid and thus manipulating passive particles. That is, by choosing a driving frequency in the propulsion regime, the swimmer may be relocated to a different point in the fluid. Then, the axis of rotation may be chosen, with a driving frequency below the first critical frequency, so that the swimmer manipulates the fluid in a desired way, without much motion of the swimmer itself. It should be noted that the values of the critical driving frequencies separating the different motion regimes depend on the body geometry, magnetization, and the strength of the applied field [15]. For the parameter values as given earlier, the values of these two critical frequencies were numerically found to be approximately $\omega_1 = 1.55$ Hz and $\omega_2 = 2.38$ Hz.

4 Particle Manipulation

4.1 Particle Dynamics in the Propulsion Regime. With this understanding of the swimmer dynamics, we now examine the system with a passive spherical particle initially located at the origin, with the artificial swimmer located at an initial position $\mathbf{X}_s = (8a, 0, 0)^{\mathbf{T}}$. The swimmer is then driven by an oscillating magnetic field of the form of Eq. (3), with $\gamma = 0$ and $\omega = 2.0$ Hz over a time span from 0 to 50 s. The resulting swimmer and particle trajectory of this simulation are shown in Figs. 2(*a*) and 2(*b*).

From these trajectories, it can be seen that the swimmer's rotational motion causes it to translate in the positive z-direction. Furthermore, the rotational velocity field produced by the swimmer causes the passive spherical particle to move in a circular path about the swimmer in the plane orthogonal to the direction of rotation and swimmer motion, with very little motion out of that plane. For this reason, the swimmer tends to move away from the passive particle, and thus, the fluid velocity field produced by the swimmer tends to decay in the vicinity of the particle. This effect is illustrated in Figs. 2(*c*) and 2(*d*). Figure 2(*c*) shows that as time progresses, the distance between the swimmer and the sphere grows larger, as the swimmer moves out of the xy-plane. Figure 2(*d*) shows the components of particle velocity throughout the simulation. From this, we see that the z-component of the particle velocity oscillates about zero for the entirety of the simulation, while the x and y components tend toward zero as the swimmer moves away from the particle. For this reason, it becomes difficult to generate significant particle motion with a swimmer operating in this regime, as the swimmer will typically tend to move away from the particle.

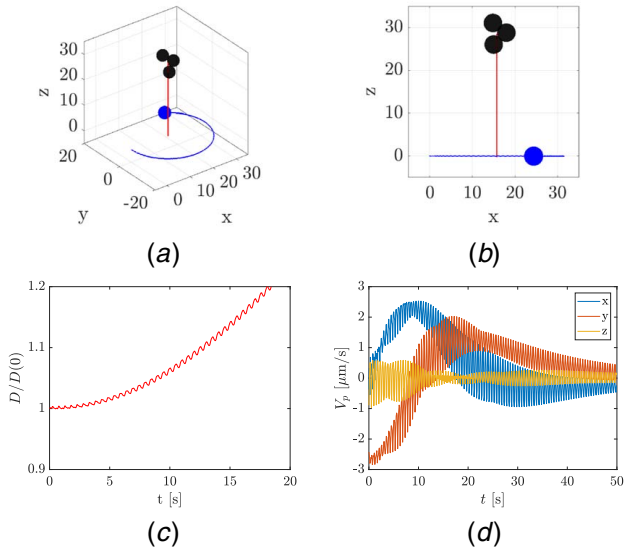

Fig. 2 (*a*) and (*b*) Trajectories of the microswimmer and passive particle when driven at $\gamma = 0$ and $\omega = 2.0$ Hz, which falls in the propulsion regime. Distances shown are given in μm. (*c*) Distance between the swimmer and the particle as a function of time. (*d*) Components of the particle's velocity, represented in the spatially fixed frame of reference.

4.2 Particle Dynamics in the Tumbling Regime. Seeing that the swimmer tends to move away from the passive particle when operating at a frequency in the propulsive regime motivates us to examine the motion of a particle as the swimmer is driven by a magnetic field rotating at a frequency below the first critical frequency. In this regime, the magnetic moment vector of the swimmer still tends to follow the rotating magnetic field, resulting in a rotating motion of the swimmer body. However, this motion is not enough to provide the body with a net translation, so the swimmer tends to rotate, or tumble, in place without much net motion.

To contrast the tumbling/spinning motion of the microswimmer with the translational motion, a simulation is done with the same initial condition as in the simulation described in Sec. 4.1, still with a magnetic field angle of $\gamma = 0$, but with a driving frequency of $\omega = 1.0$ Hz. This falls in the tumbling regime, as shown in Fig. 1(*b*). The resulting trajectories over a 50-s simulation with this input are shown in Figs. 3(*a*) and 3(*b*). The corresponding distance between the particle and the swimmer is plotted and shown in Fig. 3(*d*).

From the trajectory, it can be seen that the swimmer rotates nearly in place, with only a small amount of translation out of the xz-plane. The rotational motion of the artificial swimmer's body generates a rotational velocity field in the fluid that is similar to that generated by a rotlet. This rotational velocity of the fluid causes the passive spherical particle to translate in the xy-plane. Comparing the trajectory in Fig. 2 to the trajectory of Fig. 3, it can be seen that the sphere travels farther along its circular arc for the case of the swimmer in

Downloaded from http://asmedigitalcollection.asme.org/lettersdynsys/article-pdf/1/1/011016/6519920/aldsc_1_1_011016.pdf by Clemson University user on 16 November 2021

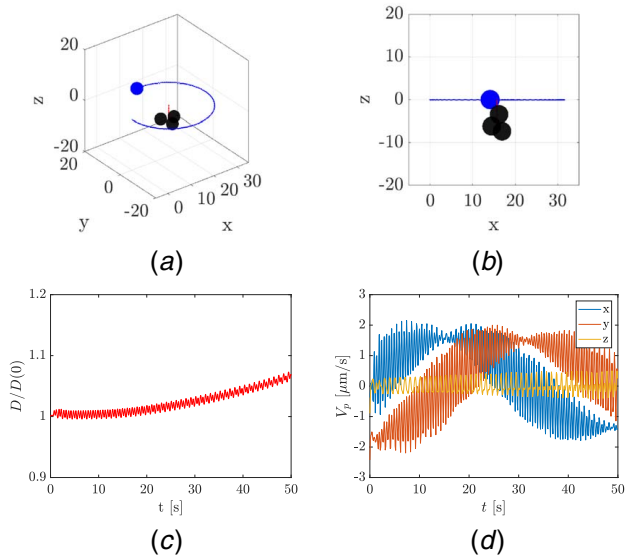

Fig. 3 (*a*) and (*b*) Trajectories of the microswimmer and passive particle when driven at $\gamma = 0$ and $\omega = 1.0$ Hz, which falls in the tumbling regime. Distances shown are given in μm. (*c*) Distance between the swimmer and the particle as a function of time. (*d*) Components of the spherical particle's velocity, represented in the spatially fixed frame of reference.

the tumbling regime. The reason behind this is as follows. When the swimmer and the particle lie in the same plane (the *xy*-plane here), the sphere's velocity is higher when the swimmer moves in the propulsive regime than when it moves in the tumbling regime. When the swimmer moves in the propulsive regime, it tends to translate out of this plane and away from the particle, whereas in the tumbling regime, the swimmer stays near to this plane throughout the simulation. For this reason, the velocity of the sphere does not decay nearly as rapidly in the tumbling case, as the distance between the particle and the sphere grows much more slowly. Both of these findings can be observed in Figs. 3(*c*) and 3(*d*).

4.3 Control by Piecewise Steady Inputs. In the previous two simulations shown, neither of the applied inputs resulted in consistent, significant propulsion for both the passive particle and the artificial swimmer. When the swimmer is driven in the tumbling regime, the particle exhibits significant motion, moving in a circular arc about the swimmer. However, not much net translation is achieved, as the particle tends to return to its original position. In the propulsive regime, the swimmer exhibits significant propulsion, translating in the direction of magnetic field rotation, but it tends to move away from the particle, resulting in small particle displacement. With this in mind, we seek to consider a sequence of driving frequencies ω and directions γ to steer both the swimmer and the particle in a desired direction.

To accomplish this, the task is broken into phases in which the swimmer is to be moved and phases in which the passive particle is to be moved. To move the swimmer, the magnetic field's axis of rotation is oriented along the desired direction and a field rotation frequency should be chosen below the step-out frequency, but above the tumbling-propulsion transition frequency. To move the passive particle, the magnetic field is oriented in a direction perpendicular to the desired direction of motion, and a frequency is chosen to place the swimmer in the tumbling regime. To illustrate this, we simulate the system with a passive particle initially located at the origin and the artificial swimmer initially located at the position $\mathbf{X}_s = (0, -10a, 0)^{\mathsf{T}}$. With this, we choose a sequence of inputs γ and ω in a piecewise constant manner with the goal of steering the swimmer in the positive z direction of the spatially fixed reference frame. More specifically, for one interval of time, we choose an input of $\omega = 1$ Hz so that the swimmer will undergo negligible translational motion and $\gamma = \pi/2$ rad, so that the magnetic field axis of rotation is aligned with the positive x-direction of the spatially fixed frame. This rotation causes the particle to move in a circular arc about the swimmer in the yz-plane. This motion is then halted before the sphere reaches the top of this circle and begins to undergo motion in the negative z-direction. Once this motion has been completed, a new control input is selected and held constant over a time interval, this time chosen with the objective of moving the swimmer in the positive z-direction. For this, the inputs $\omega = 2$ Hz and $\gamma = 0$ rad are chosen, so that the artificial swimmer moves in the propulsive regime along an axis oriented in the positive z-direction. This motion is carried out until the artificial swimmer moves past the spherical particle in the positive z direction, but not so long that the particle lies outside of the range of influence of the artificial swimmer's velocity field. At the completion of these two time intervals, both the swimmer and the particle will have achieved a net translation in the positive z direction. This cycle can thus be applied iteratively to achieve a larger net displacement. A trajectory resulting from such an input is generated and shown in Fig. 4. The inputs γ and ω applied here are as described earlier and as displayed in Figs. 4(*c*) and 4(*d*). Here, the lengths of time intervals are chosen somewhat arbitrarily and differ in order to illustrate differences in the resulting motions.

This simulation shows that translation of both the particle and the artificial swimmer in the positive z-direction can be achieved using the sequence of inputs as described earlier. This is emphasized in Fig. 4(*e*), which shows the z position of both bodies as a function of time throughout the simulation. This demonstrates precisely how each of the control inputs leads to a translation of the

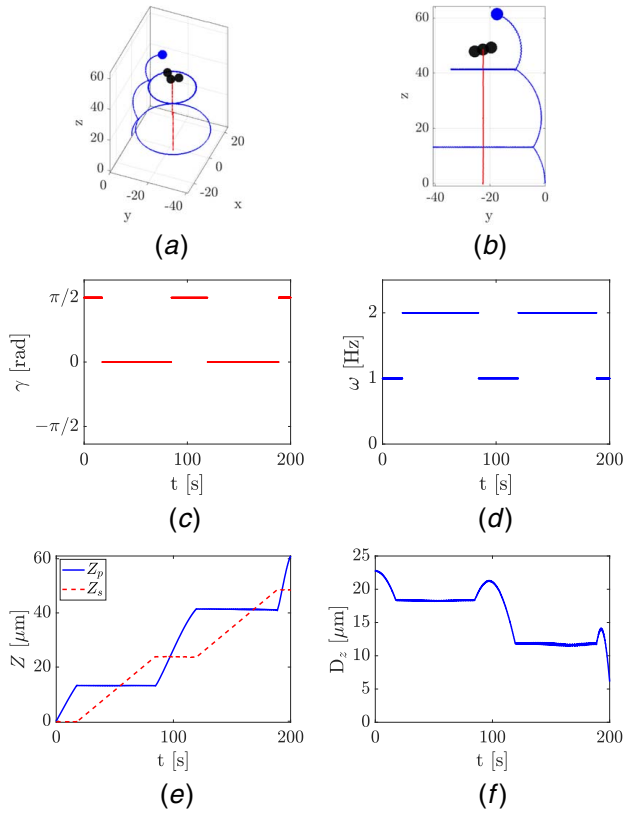

Fig. 4 (*a*) and (*b*) Trajectories of the magnetically driven swimmer and passive spherical particle in response to a control input that switches between piecewise constants, as described in Sec. 4.3. Distances shown are given in μm. (c) and (*d*) Control inputs γ and ω. (*e*) Position in the *z*-direction of the swimmer and the particle respectively over time. (*f*) Distance D_z from the desired direction of swimmer motion.

Downloaded from http://asmedigitalcollection.asme.org/lettersdynsys/article-pdf/1/1/011016/6519920/aldsc_1_1_011016.pdf by Clemson University user on 16 November 2021

swimmer or the sphere. Furthermore, since the choice of translation in the z-direction was arbitrary in this simulation, this indicates that motion of these bodies may be achieved in any direction by using a comparable algorithm.

While this simulation clearly demonstrates that the particle and the swimmer may be moved together, it also shows that the distance between the particle and the swimmer's axis of rotation may be changed. That is, there exists a sequence of inputs that allows the particle to be driven radially inward or outward from the swimmer. This can be seen by examining the distance of the particle from the axis representing the desired propulsion direction. Here, we denote this distance by D_z and show it in Fig. 4(f) as a function of time. While the trajectories in Figs. 2 and 3 show that this in-plane distance typically remains constant for a constant input, we have shown that by combining these inputs in a piecewise constant manner, this radial distance can be reduced. Further, due to the linearity and time reversibility of low Reynolds number locomotion, this indicates that the radial distance may also be enlarged by applying the time-reversed version of this input.

5 Conclusion

Artificial microswimmers have many potential applications in the biomedical field. Magnetically driven microswimmers are of particular interest, as they present the capability of being controlled remotely. In this work, we examine how a magnetically actuated artificial microswimmer may be used to contactlessly manipulate a passive spherical particle with a size quantified on a comparable length scale. We have outlined an algorithm for controlling the motion of the passive particle by adjusting the orientation and frequency of the magnetic field's rotation. It has been shown that motion of both the swimmer and the a passive spherical particle may be achieved in an arbitrary direction through a sequence of magnetic field inputs in which the direction and frequency are held constant for fixed intervals of time. Our simulations also show that the particle may be driven radially inward or outward from the artificial swimmer through certain sequences of inputs. These results imply that such a swimmer and particle may be driven to any arbitrary position and configuration using the methods proposed herein. Therefore, these results imply controllability of the system and thus may be extended and implemented to achieve more complex path planning goals. While in the past the controllability of idealized systems of singularities was investigated, for instance, in Refs. [25–27], this paper is one of the first to investigate the controllability of the interaction of a cargo particle via the locomotion of a realistic artificial microswimmer.

References

[1] Nelson, B. J., Kaliakatsos, I. K., and Abbott, J. J., 2010, "Microrobots for Minimally Invasive Medicine," Annu. Rev. Biomed. Eng., **12**(1), pp. 55–85.

[2] Patra, D., Sengupta, S., Duan, W., Zhang, H., Pavlick, R., and Sen, A., 2013, "Intelligent, Self-Powered, Drug Delivery Systems," Nanoscale, **5**(4), pp. 1273–1283.

[3] Hunter, E., Brink, E., Steager, E., and Kumar, V., 2018, "Toward Soft Micro Bio Robots for Cellular and Chemical Delivery," IEEE Rob. Automat. Lett., **3**(3), pp. 1592–1599.

[4] Zhang, L., Abbott, J. J., Dong, L., Kratochvil, B. E., Bell, D., and Nelson, B. J., 2009, "Artificial Bacterial Flagella: Fabrication and Magnetic Control," Appl. Phys. Lett., **94**, p. 064107.

[5] Cheang, U. K., Meshkati, F., Kim, D., Kim, M. J., and Fu, H. C., 2014, "Minimal Geometric Requirements for Micropropulsion Via Magnetic Rotation," Phys. Rev. E, **90**, p. 033007.

[6] Chautems, C., Zeydan, B., Charreyron, S., Chatzipirpiridis, G., Pané, S., and Nelson, B. J., 2017, "Magnetically Powered Microrobots: A Medical Revolution Underway?" Eur. J. Cardio-Thorac., **55**(3), pp. 405–407.

[7] Loget, G., and Kuhn, A., 2011, "Electric Field-Induced Chemical Locomotion of Conducting Objects," Nat. Mater., **2**, p. 535.

[8] Ahmed, D., Lu, M., Nourhani, A., Lammert, P. E., Stratton, Z., Muddana, H. S., Crespi, V. H., and Huang, T. J., 2015, "Selectively Manipulable Acoustic-Powered Microswimmers," Sci. Rep., **5**(1), p. 9744.

[9] Camacho-Lopez, M., Finkelmann, H., Palffy-Muhoray, P., and Shelley, M., 2004, "Fast Liquid-Crystal Elastomer Swims Into the Dark," Nat. Mater., **3**(5), pp. 307–310.

[10] Mirkovic, T., Zacharia, N. S., Scholes, G. D., and Ozin, G. A., 2010, "Fuel for Thought: Chemically Powered Nanomotors Out-Swim Nature's Flagellated Bacteria," ACS Nano, **4**(4), pp. 1782–1789.

[11] Solovev, A., Xi, W., Gracias, D. H., Harazim, S. M., Deneke, C., Sanchez, S., and Schmidt, O. G., 2012, "Self-Propelled Nanotools," ACS Nano, **6**(2), pp. 1751–1756.

[12] Happel, J., and Brenner, H., 1983, *Low Reynolds Number Hydrodynamics*, Springer, New York.

[13] Kim, S., and Karrila, S. J., 2005, *Microhydrodynamics: Principles and Selected Applications*, Dover Publications, Mineola, NY.

[14] Meshkati, F., and Fu, H., 2014, "Modeling Rigid Magnetically Rotated Microswimmers: Rotation Axes, Bistability, and Controllability," Phys. Rev. E, **90**(6), p. 063006.

[15] Morozov, K. I., Mirzae, Y., Kenneth, O., and Leshansky, A. M., 2017, "Dynamics of Arbitrary Shaped Propellers Driven by a Rotating Magnetic Field," Phys. Rev. Fluids, **2**(4), p. 044202.

[16] Buzhardt, J., and Tallapragada, P., 2020, "Optimal Trajectory Tracking for a Magnetically Driven Microswimmer," Proceedings of the American Control Conference, Denver, CO, July 1–3.

[17] Brady, J. F., and Bossis, G., 1988, "Stokesian Dynamics," Annu. Rev. Fluid Mech., **20**(1), pp. 111–157.

[18] Durlofsky, L., Brady, J. F., and Bossis, G., 1987, "Dynamic Simulation of Hydrodynamically Interacting Particles," J. Fluid Mech., **180**(1), pp. 21–49.

[19] Swan, J. W., Brady, J. F., and Moore, R. S., ChE 174, 2011, "Modeling Hydrodynamic Self-Propulsion With Stokesian Dynamics. Or Teaching Stokesian Dynamics to Swim," Phys. Fluids, **23**(7), p. 071901.

[20] Buzhardt, J., and Tallapragada, P., 2019, "Dynamics of Groups of Magnetically Driven Artificial Microswimmers," Phys. Rev. E, **100**, p. 033106.

[21] Goldstein, H., 1980, *Classical Mechanics*, Addison-Wesley, Boston, MA.

[22] Ghosh, A., Paria, D., Singh, H. J., Venugopalan, P. L., and Ghosh, A., 2012, "Dynamical Configurations and Bistability of Helical Nanostructures Under External Torque," Phys. Rev. E, **86**, p. 031401.

[23] Zhang, L., Petit, T., Lu, Y., Kratochvil, B. E., Peyer, K. E., Pei, R., Lou, J., and Nelson, B. J., 2010, "Controlled Propulsion and Cargo Transport of Rotating Nickel Nanowires Near a Patterned Solid Surface," ACS Nano, **4**(10), pp. 6228–6234.

[24] Man, Y., and Lauga, E., 2013, "The Wobbling-to-Swimming Transition of Rotated Helices," Phys. Fluids, **25**(7), p. 071904.

[25] Or, Y., Zhang, S., and Murray, R., 2011, "Dynamics and Stability of Low-Reynolds-Number Swimming Near a Wall," SIAM J. Appl. Dyn. Syst., **10**(3), pp. 1013–1041.

[26] Buzhardt, J., Fedonyuk, V., Sudarsanam, S., and Tallapragada, P., 2018, "Controllability of a Pair of Swimming Microrotors in a Bounded Domain at Low Reynolds Number," Proceedings of the ASME 2018 Dynamic Systems and Control Conference, Sept. 30–Oct. 3, Atlanta, GA.

[27] Buzhardt, J., Fedonyuk, V., and Tallapragada, P., 2018, "Pairwise Controllability and Motion Primitives for Micro-Rotors in a Bounded Stokes Flow," Int. J. Intell. Robot. Appl., **2**(4), pp. 454–461.

Downloaded from http://asmedigitalcollection.asme.org/lettersdynsys/article-pdf/1/1/011016/6519920/aldsc_1_1_011016.pdf by Clemson University user on 16 November 2021